HIGH-POWER RF TRANSMISSION

R.K. Cooper *
Los Alamos National Laboratory, New Mexico, USA

R.G. Carter
Lancaster University, Lancaster, U.K

Abstract
We deal primarily with the practice, as opposed to the theory, of high-power RF transmission systems. The emphasis is on commercially available power transmission components, with an explanation of their functioning.

1 INTRODUCTION

This paper discusses the means of transmission of RF power from the source to the accelerating structure or other load. The discussion cannot be comprehensive due to limitations of space, but the intention is to give a discussion in sufficient depth that the reader will have a feeling for what is really involved in transmitting high powers of RF. At a minimum the reader should feel comfortable picking up a manufacturer's catalogue and understanding what it is that all those devices do.

2 CHOOSING THE TRANSMISSION LINE

The first choice that has to be made in putting together a transmission system is that of selecting what kind of transmission line to use. There are really only two choices: coaxial line and waveguide. For the waveguide one can choose between rectangular, elliptical, or circular waveguides. Only the rectangular waveguide is discussed here, since it is by far the most common choice and has the greatest availability of circuit devices. Figure 1 shows the nomenclature used to described coaxial lines and rectangular waveguides.

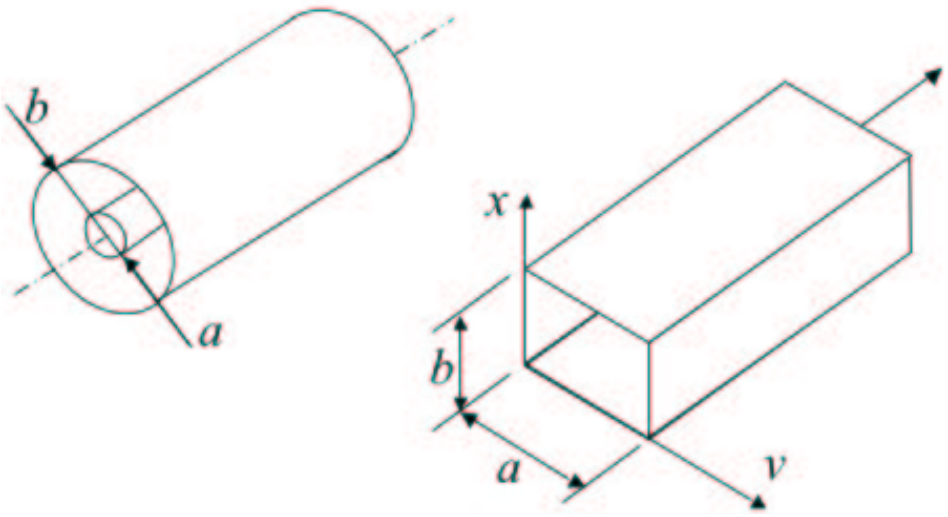

Fig. 1: Coaxial line and rectangular waveguide

* *Work supported by the US Department of Energy, Office of High Energy and Nuclear Physics.*

2.1 Coaxial line

The coaxial transmission line supports a TEM mode which has no cut-off frequency, that is, coax can be used down to d.c. This mode, in which the electric field is radial and the magnetic field azimuthal, has phase velocity and characteristic impedance given by

$$\nu_{\rm p} = c/\sqrt{\varepsilon_{\rm r}} \ , \tag{1}$$

$$Z_0 = 60 \ \ln(b/a) \ , \tag{2}$$

where c is the velocity of light in free space and $\varepsilon_{\rm r}$ is the relative permittivity of the material filling the space between the conductors. For high powers it is usual to use air-spaced lines to minimize the losses, but these require the use of dielectric spacers to support the inner conductor, as shown in Fig. 2.

Fig. 2: Typical high-power coaxial components

Coaxial transmission lines for high-power transmission are commonly available in 50 Ω and 75 Ω characteristic impedances, the former representing a compromise between breakdown field strength and power handling capacity, and the latter being selected for minimum attenuation. The ratio b/a is fixed by the characteristic impedance of the line at 2.3 for the 50 Ω line and 3.49 for the 75 Ω line. Propagation on a coaxial line is as $\exp j(\omega t - \gamma z)$ where $\gamma = \alpha + j\,\beta$. The loss parameter is given by

$$\alpha_{\rm coax} = \frac{1}{2\zeta_0 \log(b/a)} \left(\frac{R_{\rm a}}{a} + \frac{R_{\rm b}}{b} \right) \ , \tag{3}$$

where $R_{\rm a}$ and $R_{\rm b}$ are the surface resistances of the outer and inner conductors, respectively, and ζ_0 is the wave impedance of free space (= 377 Ω). The large coaxial transmission lines used for high-power transmission may use copper for the inner conductor and aluminium for the outer conductor to save

weight. The use of aluminium as the outer conductor increases the transmission losses by about 10%. The average power carried on a coaxial line is related to the peak electric field by

$$\bar{P}_{\text{coax}} = \frac{E_0^2 a^2}{\zeta_0} \pi \log\left(\frac{b}{a}\right) \quad . \tag{4}$$

The derivations of Eqs. (2), (3) and (4) are given in Appendix A. It is customary to assume that the peak electric field is the breakdown electric field strength in dry air at standard pressure and temperature, 3 MV/m. It must be remembered that this figure provides no margin of safety and that allowances must be made for changes with altitude, humidity and for the presence of dust particles in the air.

Higher-order modes (TE and TM modes) can propagate in coax at higher frequencies, and one wants to avoid these modes because mode conversion from TEM to TE or TM modes represents a source of power loss. The cut off wavenumber for the mode with the lowest cut off frequency, the TE_{11} mode, is approximately given by

$$k_c^2 (b+a)^2 \approx 4 \left[1 + \frac{1}{3}\left(\frac{b-a}{b+a}\right)^2\right] \quad . \tag{5}$$

As a numerical example, let us consider a 500 MHz power system using a rigid, air-filled, 75 Ω aluminum 14 inch outer diameter outer conductor transmission line. The radii of the outer and inner conductors are then a = 51 mm and b = 178 mm. Neglecting higher order waveguide mode effects and $\sigma_{\text{Cu}} = 5.8 \times 10^7$ mhos/m and $\sigma_{\text{Al}} = 3.5 \times 10^7$ mhos/m, so that the surface resistances are $R_a = (\sigma_{\text{Cu}}\delta_{\text{Cu}})^{-1}$ = 5.8×10^{-3} Ω per square and $R_b = (\sigma_{\text{Al}}\delta_{\text{Al}})^{-1} = 7.5 \times 10^{-3}$ Ω per square, the attenuation constant is

$$\alpha_{\text{coax}} = \frac{1}{2 \cdot 377 \cdot 1.25}\left(\frac{5.8 \times 10^{-3}}{0.051} + \frac{7.5 \times 10^{-3}}{0.178}\right) = 1.66 \times 10^{-4}\,\text{m}^{-1} \tag{6}$$

The power handling capacity is (with no safety factor or allowance for variation of breakdown field strength due to elevation, say)

$$\bar{P}_{\text{coax,max}} = \frac{(3 \times 10^6)^2 \pi (0.051)^2}{377} 1.25 = 244\ \text{MW} \tag{7}$$

The cut-off wavenumber is obtained from Eq. (5) as

$$k_{\text{c}}^2 \approx \frac{4\left[1 + \frac{1}{3}\left(\frac{17.8-5.10}{17.8+5.10}\right)^2\right]}{(17.8+5.10)^2} = 8.41 \times 10^{-3}\,\text{cm}^{-2} \quad . \tag{8}$$

Whence

$$k_{\text{c}}^2 = 0.092\,\text{cm}^{-1} \tag{9}$$

and

$$f_{\text{c}} = \frac{c}{2\pi} k_{\text{c}} = 439\ \text{MHz} \quad . \tag{10}$$

Thus we would not want to use this particular coaxial line much above 400 MHz, for example. Raising the TE_{11} cut-off frequency to 550 MHz for the same characteristic impedance would require a = 41 mm and b = 142 mm, yielding α = 2.1×10^{-4} m^{-1} and a maximum average power of 155 MW.

2.2 Rectangular waveguide

Standard rectangular waveguides have aspect ratios close to 2:1, but reduced-height waveguides are sometimes used for special purposes. The propagation constant in rectangular waveguide is given by

$$\beta^2 = \beta_0^2 - k_{\rm c}^2 \ , \tag{11}$$

where the cut-off wavenumber $k_{\rm c} = \pi/a$ and the cut-off frequency $f_{\rm c} = c/2a$ for the lowest mode of propagation. In this mode, the $\rm TE_{10}$ (or $\rm H_{10}$) mode, the electric field is normal to the broad wall and the magnetic field is parallel to the broad wall. Assuming that $b = a/2$ the attenuation constant is found to be

$$\alpha_{\rm wg} = \frac{2\,R_s\left[1 + (f_{\rm c}/f)^2\right]}{\alpha\zeta_0\left[1 - (f_{\rm c}/f)^2\right]^{0.5}} \tag{12}$$

and the maximum power is

$$\bar{P}_{\rm wg} = \frac{E_0^2 a^2}{\zeta_0}\, ab\,\sqrt{1 - (f_{\rm c}/f)^2} \ . \tag{13}$$

The derivations of Eqs. (12) and (13) are given in Appendix B. The power-handling capacity of a transmission line decreases with increasing altitude [1] because the breakdown field strength is a decreasing function of pressure. This is sometimes counteracted by pressurizing the waveguide. Thus, for example, the 1300 MHz RF power system of the Los Alamos (elevation 7000 feet = 2134 m) free-electron laser linac is pressurized to 10^{-12} psig with $\rm SF_6$. Such pressurization is the exception rather than the rule. For one thing, pressurization may cause the waveguide to deform, thus altering the propagation constant, which might then become a function of atmospheric pressure. (To counter this effect the waveguide manufacturers produce heavy-wall high-pressure waveguides.) It is, however, fairly common practice to pressurize the waveguide system with approximately 1 psig or so of dry nitrogen, to serve as a monitor for the tightness of the system, under the philosophy that if there are no air leaks there will be no RF leaks. This has the added advantage of ensuring that the accelerator structure is filled with dry nitrogen, rather than atmospheric air, if a high-power window should fail. That significantly reduces the time needed to recommission the accelerator following the failure.

Higher order waveguide modes are also a consideration in using rectangular waveguides. For the conventional choice of a $2:1$ aspect ratio in the transverse dimensions, the first higher order mode is the $\rm TE_{20}$ mode ($\rm H_{20}$ mode), for which the cut-off frequency is just twice the cut-off frequency of the dominant $\rm TE_{10}$ mode ($\rm H_{10}$ mode). Common practice is to use a rectangular waveguide with a $\pm 20\%$ bandwidth about a centre frequency which is 1.5 times the waveguide cut-off frequency. Roughly put, one operates in a band from approximately 1.25 f_c to 1.90 f_c. Table 1 shows the standard waveguides for high-power transmission in the frequency range commonly used for particle accelerators.

In the grey area around 200 to 400 MHz, where one might want to choose either coaxial transmission line for its more compact size, or a waveguide for its lower attenuation, one must bear in mind both attenuation and power-handling capacity.

For the high-power transmission system discussed previously but using a WR1800 waveguide made of aluminium, with a = 18 inches = 0.457 m, the attenuation constant is

$$\alpha_{\rm wg} = \frac{2 \cdot 7.5 \times 10^{-3}\left[1 + (327.9/500)^2\right]}{0.457 \cdot 377\ \left[1 - (327.9/500)^2\right]^{0.5}} = 1.65 \times 10^{-4}\,{\rm m}^{-1} \tag{14}$$

Table 1: Standard waveguide characteristics

Waveguide designation	**Inside dimensions (inches)**	**TE_{10} mode operating Range (MHz)**	**Cut-off frequency (MHz)**	**Cut-off wavelength (cm)**
WR2300	23.0×11.5	320–490	256	116.84
WR2100	21.0×10.5	350–530	281	106.68
WR1800	18.0×9.0	410–625	328	91.44
WR1500	15.0×7.5	490–750	393	76.20
WR1150	11.5×5.75	640–960	513	58.42
WR975	9.75×4.875	750–1120	605	49.53
WR770	7.7×3.85	960–1450	766	39.12
WR650	6.5×3.25	1200–1700	908	33.02

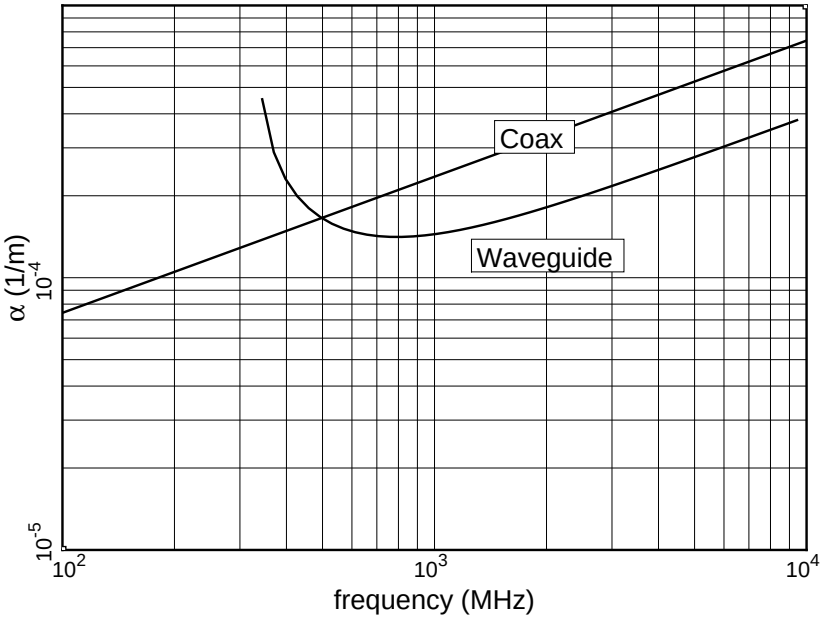

Fig. 3: Attenuation constants for a 14 inch coaxial line and for WR1800 waveguide

and the maximum power is

$$\bar{P}_{\text{wg,max}} = \frac{(3 \times 10^6)^2 \, 0.457 \cdot 0.229}{4.377} \sqrt{1 - (327.9/500)^2} = 471 \text{ MW} \ . \tag{15}$$

Thus at 500 MHz choosing a waveguide over a coax line is fairly clear cut. In order to avoid higher order waveguide mode losses, the diameter of the coax must be reduced, leading to higher attenuation and lower power-handling capacity as shown above. For short distances of transmission, however, the higher losses of coaxial transmission lines may be acceptable. Figure 3 shows attenuation versus frequency for a 14-inch coaxial line and a WR1800 waveguide. The figure is intended to show the frequency dependence of both coaxial line and waveguide and should not be interpreted as implying a choice between these two transmission lines. The attenuation constant α of a coaxial line increases with increasing frequency as the square root of the frequency, because of the surface resistance term, which contains a skin-depth factor. The attenuation constant for a waveguide has a more complicated frequency behaviour, as given

in Eq. (12) and shown in Fig. 3. As a function of frequency, the attenuation constant has a minimum at 2.471 f_c [2], but this frequency is not used for transmission, because several higher order modes can also propagate at the same time.

Figure 4 shows the attenuation constant α versus frequency for standard waveguides throughout their recommended frequency bands. The attenuation increases with frequency because of the decrease in the skin depth. Figure 5 shows the power-handling capacity of standard waveguides assuming a breakdown field strength of 3 MV/m.

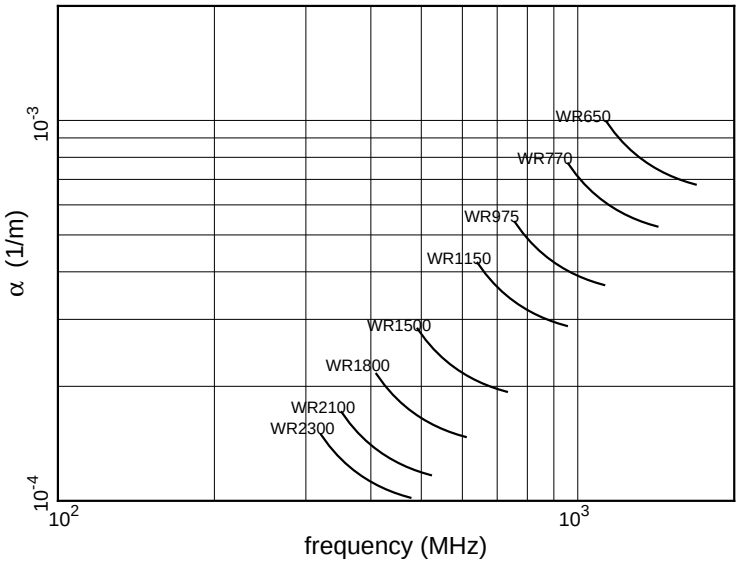

Fig. 4: Attenuation constant vs frequency for standard waveguides

Figure 6 shows a 425 MHz system set-up for evaluation of its performance. At the left is seen a klystron with its output to waveguide. Up from the klystron is a 90° mitred H-plane bend. Just before the Y-shaped circulator is a dual directional coupler. In the horizontal direction after the circulator is a 90° mitred E-plane bend. Following the bend is a broad-wall directional coupler. The operation and characteristics of these components, and more, are discussed in the remainder of this paper.

3 TWO-PORT DEVICES

3.1 Bends

Bends in waveguide systems typically leave the plane of the top (broad) waveguide wall undisturbed, or they leave the plane of the side (narrow) wall unchanged. Bends of the former type are known as H-plane bends, while the latter type are known as E-plane bends. In practice, both E-plane and H-plane bends commonly come in two forms, swept and mitred.

A swept bend forms a gradual change of direction. Figure 7 shows schematically a swept H-plane bend and a mitred H-plane bend. Swept bends tend to be rather long; a bend of two guide wavelengths in length is common and is good engineering practice. The reasoning behind this last statement is based on the observation that if two transmission lines of characteristic impedance Z_0 are connected by a transmission line of characteristic impedance Z_1, then there will be no reflection arising from the change of impedance if the length of the intermediate line is an integral number of half guide wavelengths long. That is, the impedance seen looking into the first junction between Z_0 and Z_1 is, assuming the second Z_0 line is properly terminated and the length of the intermediate line is L,

$$Z_{\text{in}} = \frac{Z_0 \cos \beta L + j Z_1 \sin \beta L}{j_0 (Z_0/Z_1) \sin \beta L + \cos \beta L} \quad , \tag{16}$$

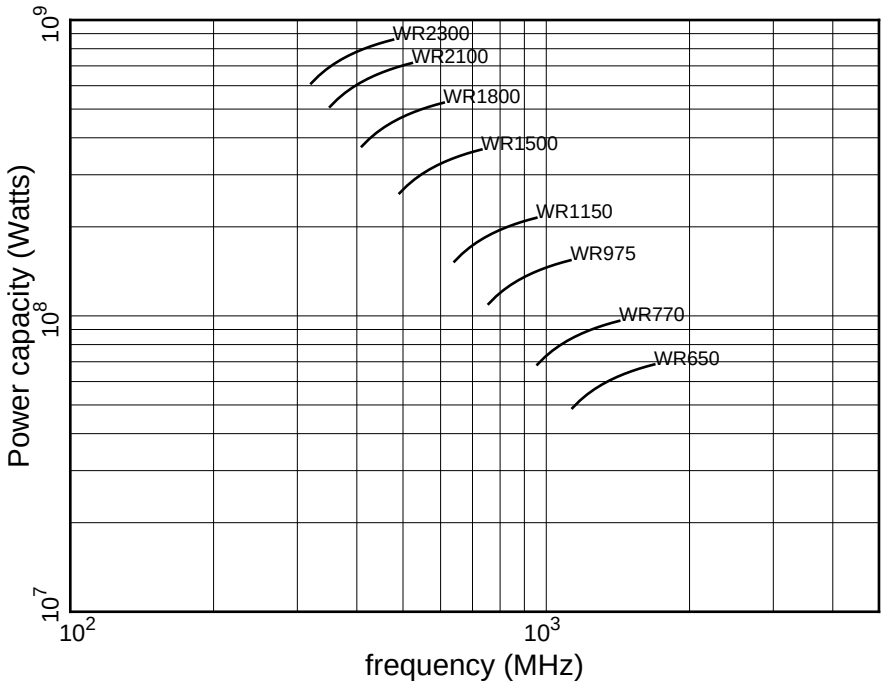

Fig. 5: Waveguide power handling capacity at a beakdown voltage of 3 MV/m

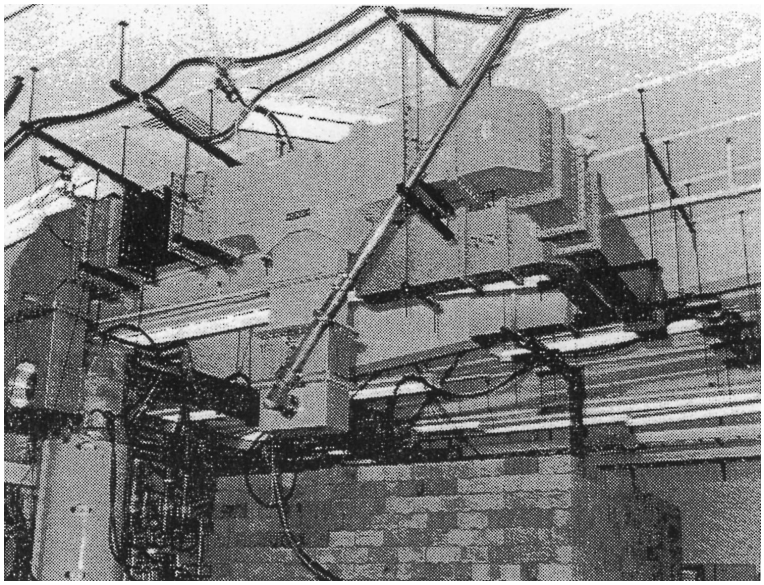

Fig. 6: A 425 MHz system set up for evaluation

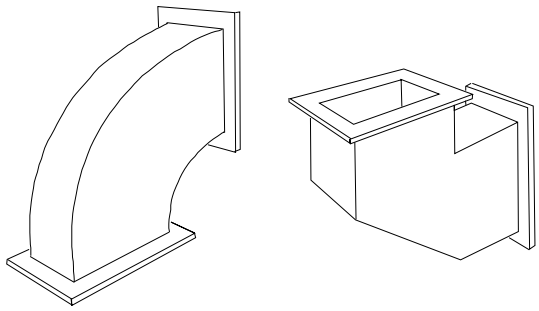

Fig. 7: Outline of a swept H-plane bend (left) and a mitred H-plane bend (right)

which will have the value Z_0 whenever βL is a multiple of π.

A mitred bend, on the other hand, can be quite compact, slightly longer than one electrical wavelength. A 90° H-plane bend is essentially a right-angled junction with a reflecting plane replacing the outer corner. The location of this plane is discussed in Ref. [1]. Other mitred bends have both corners replaced by 45° planes.

Commercially available swept H-plane bends have a maximum Voltage Standing Wave Ratio (VSWR, the ratio of the sum of the incident and reflected wave amplitudes to the difference of the incident and reflected amplitudes) of 1.03 over the 40% waveguide band, while the mitred bends have a maximum VSWR of 1.02, but only over a 10% band.

Essentially the same remarks can be made about the swept E-plane bends and the mitred E-plane bends as were made about the H-plane bends, including performance characteristics.

3.2 Twists and tapers

It is often the case that the plane of polarization of the electric field must be rotated by 90°. One can choose to make a gradual change (twist) of the waveguide, or one can make the change of plane in a series of discontinuous rotations. The problem with gradual changes in general is that they take up length in the transmission system. The step twist, on the other hand, accomplishes the rotation in a distance as short as three-quarters of a guide wavelength. Figure 8 shows a 90° step twist. The basic idea of the

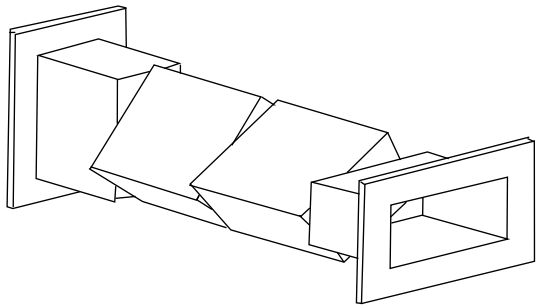

Fig. 8: Outline drawing of a 90° step twist

step twist is that the discontinuities in the orientation of the component waveguide sections should occur at one-quarter guide wavelength separation, so that reflections from the discontinuities are allowed to cancel. If we denote by θ the rotation angle between the sides of two sections of waveguide, then the reflection coefficient arising from the discontinuity will be proportional [3] to θ^2 for small enough θ. If we want to accomplish a 90° twist with, say, three rotations of angles θ_1, θ_2, and θ_1, then we would want

the reflection coefficients to be in the ratio 1:2:1 for pairwise cancellation of the reflected waves. Thus we want to have:

$$\begin{array}{ccccccc} 1 & : & 2 & : & 1 & & \\ \theta_1^2 & : & \theta_2^2 & : & \theta_1^2 & & \\ 26.4^\circ & + & 37.2^\circ & + & 26.4^\circ & = 90^\circ & . \end{array}$$

In practice these angles need to be adjusted slightly for optimum performance. One expects to obtain a VSWR resulting from reflection from a step twist of the order of 1.05 or less over a bandwidth of at least 10%. Step twists with five rotations are also available for broader-band performance and higher power-handling capacity. Other angles of twist such as 30°, 45°, and 60° are also available. The power-handling capacity of the step twist is about half that of the waveguide to which it is mated, and therefore may represent the weakest link in the transmission chain.

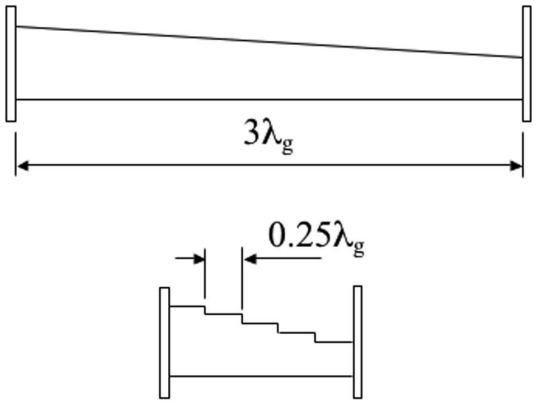

Fig. 9: Outline drawings of gradual and stepped height tapers

Where it is necessary to make a transition from standard waveguide to reduced-height waveguide we may use either a gradual or a step taper, as shown in Fig. 9. The gradual taper must have a length of at least three guide wavelengths to achieve an acceptable VSWR. The step taper, employing three or four quarter-wavelength steps, is much shorter and can be made with good VSWR if it is only to operate over a narrow band. Figure 10 shows a waveguide system with swept and mitred bends and a step transformer to reduced-height waveguide.

3.3 Windows

Since the high-power waveguide system is normally at atmospheric pressure, it is necessary to provide RF windows between the waveguide and the accelerating structure. There are, of course, similar windows on the outputs of high-power klystrons, which are an integral part of those tubes. The RF windows are often the most critical part of a high-power RF system, since their failure will cause the high vacuum system to go ‘down-to-air’, leading to the need for a lengthy period of reconditioning before the system is fully operational again.

Figure 11 shows the arrangement of a number of common types of RF window. The window is typically made from high purity alumina ceramic which is brazed into the transmission line. The simplest are those in coaxial line [Fig. 11(a) and circular waveguide Fig. 11(b)]. These have the advantage that the thermal stresses produced in the window by dielectric heating are symmetrical and that the field pattern in the ceramic matches that in the empty transmission line, avoiding mode conversion. To achieve a good match the window must either be thin, half a wavelength thick, or provided with additional matching

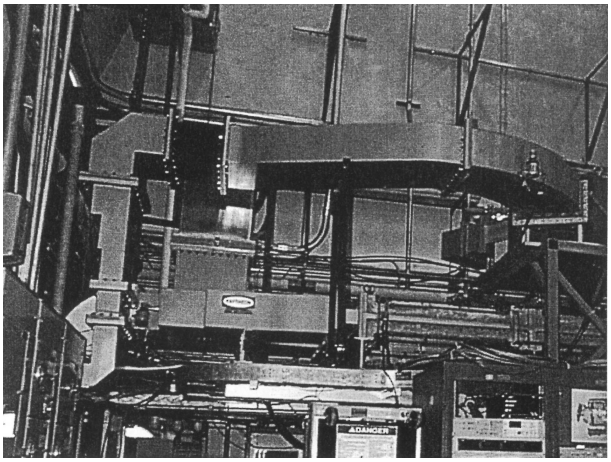

Fig. 10: Arrangement of a typical high-power waveguide system

elements. The lighthouse window [Fig. 11(c)] employs a cylindrical ceramic around the junction between a coaxial line and a waveguide. This arrangement is particularly suitable when the coupler that feeds RF power into the accelerator is in coaxial line. The creation of a window in a rectangular waveguide by fixing a rectangular piece of ceramic into the waveguide is not suitable for use at high power levels because of the stress concentrations that occur at the corners of the ceramic. A possible alternative is to use an iris window, as shown in Fig. 11(d). The iris is designed to be resonant at the centre frequency of the band of frequencies required. Additional matching elements must be used if broadband operation is required. Finally, the pill-box window [Fig. 11(e)], is essentially a circular waveguide window placed between a pair of transitions from circular to rectangular waveguide. Because the ceramic is larger than that of an iris window, the power-handling capacity is higher. With careful design a pill-box window can give a good VSWR over a band of frequencies.

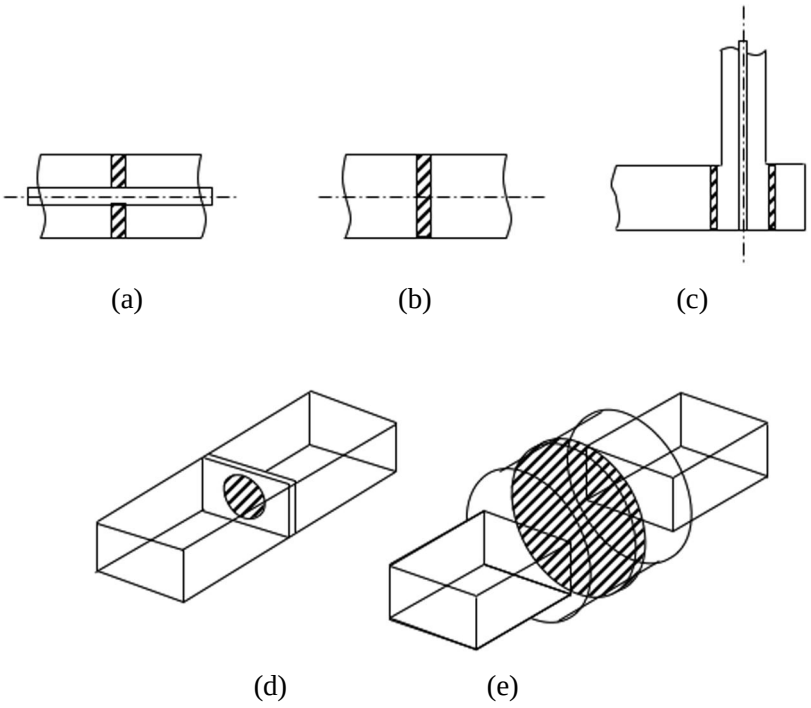

Fig. 11: Various types of RF windows

Because the consequences of window failure can be catastrophic, it is usual to take precautions against such an event. Common precautions are provision of air-blast cooling on the air side of the window, monitoring of the window temperature, and the use of double windows in series.

3.4 Mode transformers

It is sometimes necessary to couple power from one type of transmission line to another with a low VSWR. In order to achieve this, the basic principle is to try to ensure that the electric and magnetic field patterns on the two sides of the junction are roughly similar. Since the field patterns are not normally an exact match, some of the RF power is scattered into higher order modes. Provided these are cut off, no power can propagate in them and it therefore remains stored as reactive energy in the region close to the junction. The mismatch caused by this reactance can be tuned out by the addition of matching elements (posts or irises) to give a good overall VSWR. Rather different problems arise when the higher order modes can propagate because significant power can then be scattered into undesired modes. This should not normally happen at the fundamental frequency, but it can cause serious problems at harmonic frequencies. A high-power RF system always contains some harmonic power from the output of the RF source or from power induced in the accelerating structure by beam bunches. Harmonic power can cause standing waves in the waveguide and trigger waveguide breakdown.

Figure 12 shows, as an example, how power can be coupled from the TE_{10} rectangular waveguide mode to the TM_{10} circular waveguide mode (or *vice versa*). When the rectangular waveguide is terminated in a short circuit the resulting standing wave has magnetic field lines, which are approximately circular, as shown on the left of Fig. 12. These are a good match to the magnetic field in the circular waveguide. In order to match the electric field lines it is necessary to add a post to the junction, as shown on the right of Fig. 12. The dimensions of the post are adjusted to match the junction and additional matching elements can be added in either, or both, of the waveguides if necessary.

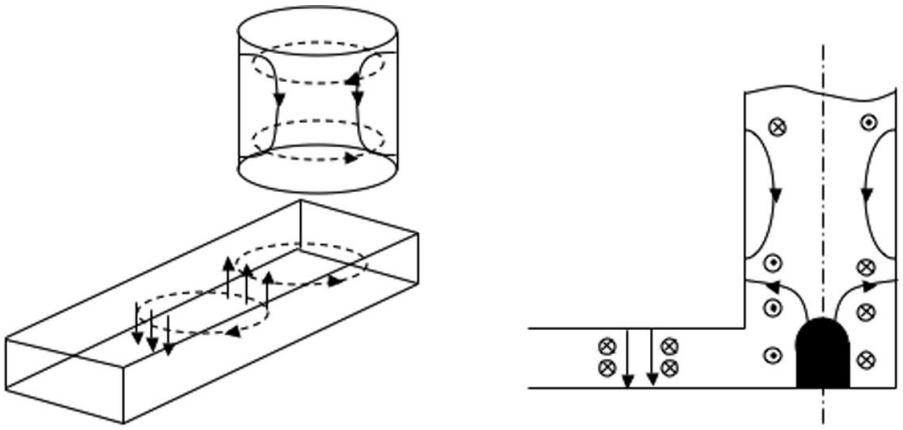

Fig. 12: Arrangement of a transition from rectangular to circular waveguide

The most common types of mode transformer are those for coupling power from a coaxial line to a rectangular waveguide. There are a number of ways of achieving this but the only ones that are really suitable for use at high power levels are the door-knob transition and the tee bar transition illustrated in Fig. 13. Note that in this case part of the problem arises from the mismatch of impedance between the waveguide (typically 200 Ω) and the coaxial line (50 Ω or 75 Ω).

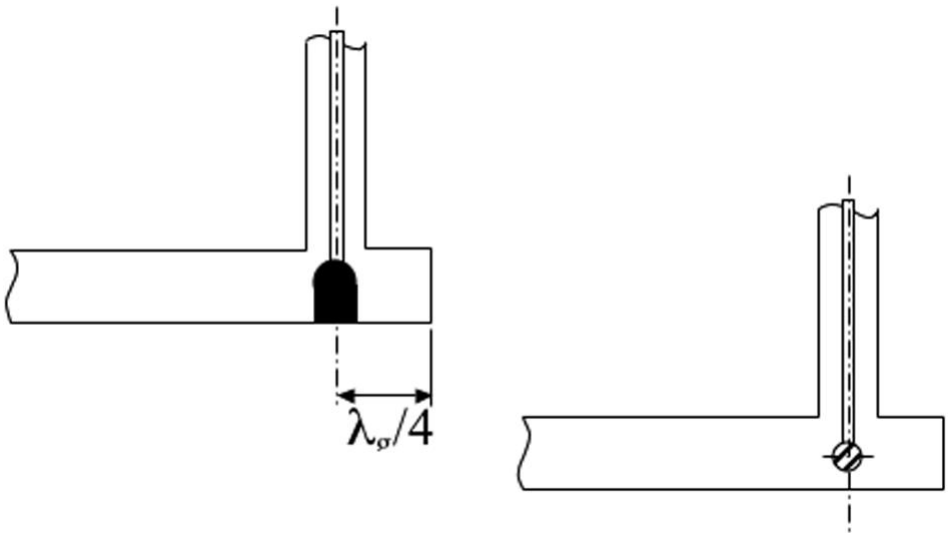

Fig. 13: Arrangements of high-power transitions from coaxial line to waveguide

4 THREE AND FOUR-PORT DEVICES

4.1 Directional couplers

In waveguide transmission systems it is often useful and necessary to couple energy from one waveguide system into another system. Such coupling might be to provide power to the second system, or to provide a measure of the power flow in the first system. Consider, first, two rectangular waveguides side by side with a common side wall, with a hole connecting the two waveguides, as shown in Fig. 14. The action of the hole can be described by considering it as a dipole radiator that is excited by the wave S_0 in the primary waveguide. The dipole radiates waves symmetrically into both waveguides as shown, with the condition that the sum of the powers emerging from the four ports is exactly equal to that in the incident wave (for a theoretical lossless device). Since the action of the hole is to couple some of the incident power to ports 3 and 4 and some power re-emerges from port 1, it follows that the wave S_{1+} must combine destructively with S_0 so that the power emerging at port 2 is reduced by the presence of the hole. By using two or more coupling holes it is possible to make devices, known as directional couplers, which couple power selectively to particular ports.

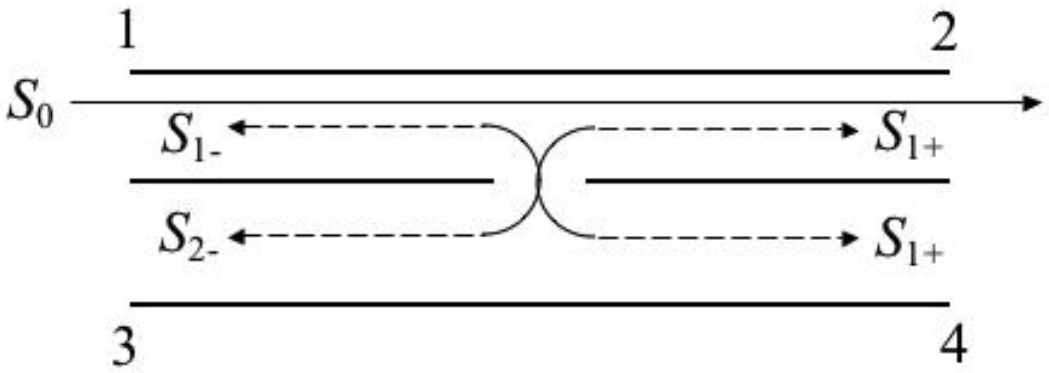

Fig. 14: Waveguides coupled by a hole in their common wall

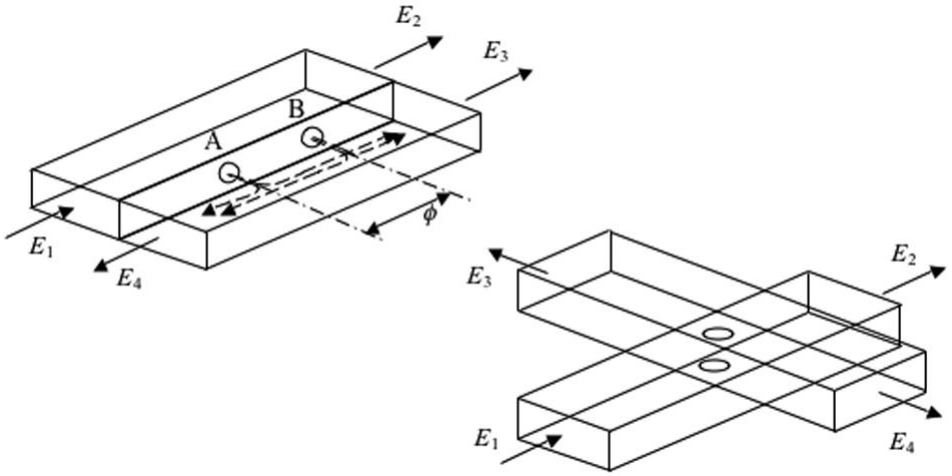

Fig. 15: Directional couplers

The principle of two common types of directional coupler is illustrated in Fig. 15. The left-hand diagram shows two waveguides coupled by a pair of identical holes in their common, narrow wall. If we treat port 1 as the input port then hole B will be excited with a phase shift ϕ relative to hole A, where ϕ is the electrical length of the guide between the holes. Thus the forward waves radiated by the two holes into the second guide are always in phase with each other and add together, and the amplitude of E_3 is non-zero. If we choose $\phi = \pi/2$ then the backward wave in the second guide radiated by hole B is in antiphase with that radiated by hole A at the plane of A and $E_4 = 0$. Thus the power input at port 1 has been divided between ports 2 and 3 in a proportion determined by the sizes of the holes. Since the device is symmetrical, the same argument can be applied to power input at any of the ports. It is important to note that, as described, this coupler works perfectly at only one frequency. The coupling can be increased and made broadband by the use of arrays of holes. For details on the theory of design of multihole couplers see Ref. [4]. The S matrix of a directional coupler has already been given in these proceedings by Caspers [5]. The coupler described is known as a 'side-wall coupler'. It is also possible to make couplers with holes in the common broad wall. Couplers for use at low power levels often have three ports, since one port is terminated in an internal matched load. This is not normally suitable for high-power use, where a four-port coupler with an external high-power load is required. The properties of a directional coupler excited at port 1 are described by

$$\text{Coupling} = 20 \log_{10} \left| \frac{E_1}{E_3} \right| \tag{17}$$

and

$$\text{Directivity} = 20 \log_{10} \left| \frac{E_3}{E_4} \right| \ . \tag{18}$$

The coupling measures the transfer of power to the second guide. For purposes of monitoring and control this is normally quite small and the coupled power is typically 30 dB or 40 dB below that in the main guide. A special case is the power divider, with 3 dB coupling, which splits the power equally between ports 2 and 3. This is examined further in Sections 4.2 and 4.3. The directivity is a measure of how close the coupler is to perfection. It is usually at least 30 dB and exceeds 40 dB for couplers designed

for measurement systems. Typical characteristics of a commercially available coupler over a bandwidth of 10% are VSWR, 1.05; directivity, 30 dB; coupling variation ±0.5 dB; coupling factor range, 6 dB to 50 dB (a fixed value of, for example, 20 dB for any individual coupler).

The diagram on the right of Fig. 15 shows the arrangement of a cross-guide coupler. These couplers do not have good broadband characteristics because they normally have only two coupling holes. The principle of operation is similar to that already described. Cross-guide couplers have the advantage of being very compact. They are particularly useful in situations where accuracy is not critical, such as in the monitoring of reflected power to detect waveguide arcs. See Ref. [6] for details of various directional coupler schemes.

In the larger waveguide sizes another form of directional coupler is available. This type of coupler, described by Klein [6], consists of a circuit loop penetrating into the waveguide top wall. The loop will have currents induced in it both by the electric field of the waveguide mode and by the magnetic field of the mode. By proper orientation and termination of the loop, the electric and magnetic currents can be made to be equal in magnitude. Then a wave in the forward direction, say, will produce a current in the loop, which is the constructive sum of the electric and magnetic currents, while a backward-travelling wave produces no current in the loop because the electric and magnetic currents cancel each other. See Ref. [7] for a circuit analysis of the operation of these loop-type couplers. These couplers are commercially available packaged singly (for power monitoring) and doubly (for reflectometer use). Typical characteristics of such couplers over a 10% bandwidth are coupling factor range, 40–75 dB (a fixed value for any particular coupler); VSWR, less than 1.05; directivity, greater than 25 dB; insertion loss, less than 0.1 dB.

4.2 The Riblet coupler

We discuss next the short-slot hybrid coupler. To quote from Harvey [7]: “The hybrid junction is a four terminal-pair device which ideally has the property that power supplied to a given terminal is divided, usually equally, between two of the three remaining terminal-pairs and nothing is coupled to the fourth terminal-pair.” The Riblet short-slot hybrid coupler [8] is one of these devices and forms the basis of a number of useful waveguide devices, such as the phase shifter and the variable attenuator. Note also that the magic tee, described below, is also a hybrid junction according to this definition. The Riblet coupler is depicted in Fig. 16. Two waveguides with a common side wall have a section of that wall removed.

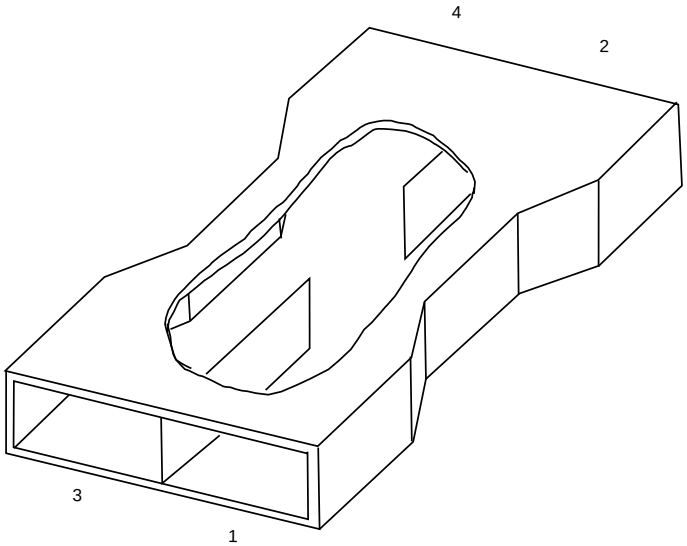

Fig. 16: Outline drawing of a Riblet coupler

Table 2

Location	**Port 1**	**Port 2**	**Port 3**	**Port 4**
Entering	E_0	0	0	0
Leaving	0	$E_0/\sqrt{2}$	0	$j\,E_0/\sqrt{2}$
Entering	0	$\rho e^{j\phi}\,E_0/\sqrt{2}$	0	$j\,\rho e^{j\phi}\,E_0/\sqrt{2}$
Leaving	0	0	$j\,\rho e^{j\phi}\,E_0$	0

In that portion of the coupler with the side wall removed there is a double-width waveguide in which both the TE_{20} mode and the TE_{10} can propagate. (The width is sometimes narrowed, as shown, to keep the H_{30} mode from propagating.) By choosing the length of the removed wall section properly, an equal division of the power incident in the first guide can result. The forward-going wave in the coupled guide has in addition a phase shift of 90°, whereas there is no backward-going wave in the coupled guide. The scattering matrix for the Riblet coupler is given by

$$S = \frac{1}{\sqrt{2}} \begin{pmatrix} 0 & 1 & 0 & j \\ 1 & 0 & j & 0 \\ 0 & j & 0 & 1 \\ j & 0 & 1 & 0 \end{pmatrix} \quad . \tag{19}$$

As an illustration of a simple application of the Riblet coupler and to introduce a form of analysis to be used later, consider using the coupler to split power equally from a source to two identical loads. The table below shows how the power is first split from port 1 equally into ports 2 and 4, how the reflected powers from the identical loads (reflection coefficient ρ, overall phase shift from coupler to load and back ϕ) re-enter the coupler at ports 2 and 4, and how the reflected powers recombine in the coupler to exit at port 3. Thus no reflected power comes out from port 1, so that the source is isolated from the load reflections.

For purposes of typography and explanation, let us consider instead of the customary S matrix definition,

$$E_{\text{scattered}} = S\,E_{\text{incident}} \quad , \tag{20}$$

where the E's are column vectors with entries representing the amplitudes of the fields at the respective ports, the transposed equation

$$\tilde{E}_{\text{scattered}} = \tilde{E}_{\text{incident}}\,\tilde{S} \quad , \tag{21}$$

where the tilde represents the transpose of the indicated quantity. Thus we have an equation relating row vectors instead of the more commonly used column vectors. If we have a wave incident only on port 1, the incident vector is given by $(E_0\ 0\ 0\ 0)$, and the scattered vector is given by

$$\begin{aligned} S &= (E_0, 0, 0, 0)\,\frac{1}{\sqrt{2}} \begin{pmatrix} 0 & 1 & 0 & j \\ 1 & 0 & j & 0 \\ 0 & j & 0 & 1 \\ j & 0 & 1 & 0 \end{pmatrix} \\ &= (0, E_0/\sqrt{2}, 0, j, E_0/\sqrt{2}) \quad . \end{aligned} \tag{22}$$

We see that each row of Table 2 above labelled 'leaving' can be obtained from the row above it labelled 'entering', simply by multiplying the entering row into the transpose of the scattering matrix.

4.3 The magic tee

H-plane and E-plane tees have already been discussed by Caspers [5] who has also given the S matrix characterization of these junctions. In high-power systems these junctions are used mainly to provide opportunities for matching loads to sources, and will not be discussed further here.

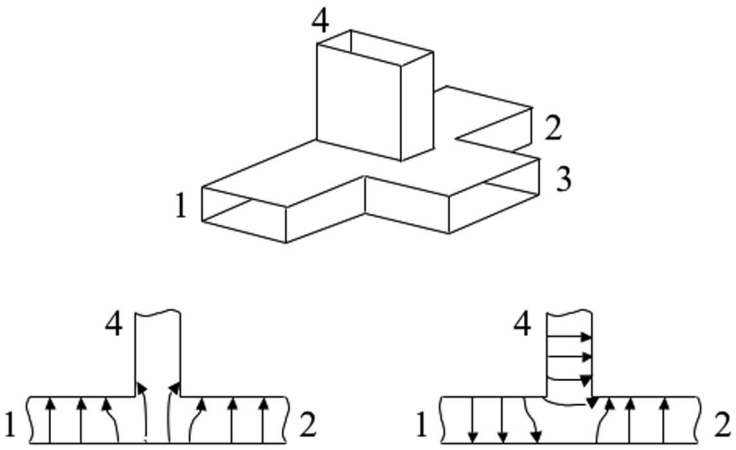

Fig. 17: Arrangement and principle of operation of a magic tee

Figure 17(top) shows the arrangement of a 'magic tee' which comprises an H arm, an E arm, and two co-linear arms. The properties of a magic tee can be illustrated simply by considering the effect of exciting ports 1 and 2 in phase and in anti-phase. When they are excited in phase (Fig. 17, left) the resulting signal is coupled to the TE10 mode of the H arm (port 3) but not to that of the E arm (port 4). When the excitation is in antiphase (Fig. 17, right) the coupling is to port 4 but not to port 3. The magic tee is therefore another example of a hybrid junction as defined in Section 4.2. Since it is a passive device, its properties must be symmetrical so that power entering at port 3 excites waves at ports 1 and 2 in phase with each other and power entering at port 4 excites outputs at ports 1 and 2 in antiphase. The scattering matrix of a magic tee is

$$S = \frac{1}{\sqrt{2}} \begin{pmatrix} 0 & 0 & 1 & 1 \\ 0 & 0 & 1 & -1 \\ 1 & 1 & 0 & 1 \\ 1 & -1 & 0 & 0 \end{pmatrix} \quad . \tag{23}$$

As an application of power splitting and combining, consider the output waveguide system of the SLAC 5045 klystron. The output power of 67 MW (peak power) exceeds the capacity of a single ceramic window, so a magic tee is used to split the power equally between the co-linear arms, the power is passed equally between two windows, and then recombined in a second magic tee.

In a load-isolation application, one may input power in the H arm, split it equally between the colinear arms, and thereby send equal power to equal loads. If one of the loads is located an electrical distance 90° further from the magic tee than the other load, then any reflection common to the two loads will combine to go up the E arm.

Commercially available magic tees for high-power application have the following typical characteristics over a 10% bandwidth: balance between the colinear arms, ± 0.1 dB; insertion loss, less than 0.1 dB; isolation of the E and H arms, 30 dB minimum; VSWR, less than 1.10. Folded magic tees are also commercially available (Fig. 18); these tees have slightly poorer characteristics than the standard magic tee, but have the advantage of a more compact structure. These tees are commonly used, for instance, in circulators (see Section 6).

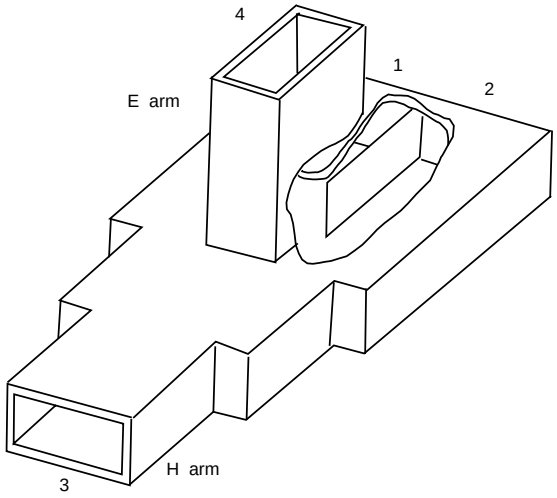

Fig. 18: A folded magic tee

5 PHASE SHIFTERS AND VARIABLE ATTENUATORS

At low power levels it is possible to make phase shifters and attenuators by placing dielectric or lossy vanes within the waveguide. At high power levels this is not possible because the vanes are incapable of handling the power required. An alternative approach that is satisfactory for use in high-power systems is to make use of the properties of hybrid junctions.

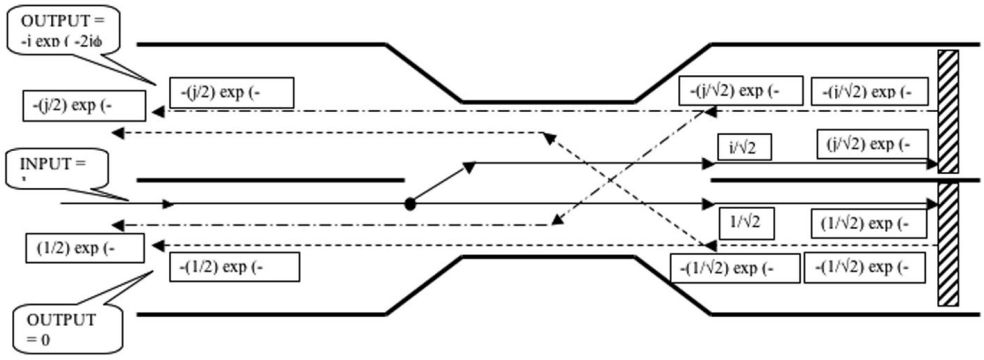

Fig. 19: A Riblet coupler with short circuit terminations

If the 'loads' of the Riblet coupler load isolation system are in fact shorts, then ρ = –1 and the result is that the action of the coupler with two identical shorts is represented by the diagram in Fig. 19. The information in the diagram can be summarized by writing

$$\begin{aligned} E_{\text{incident,port 1}} &= E_0 \\ E_{\text{outgoing,port 3}} &= -j\,E_0\,E^{j\phi} \quad . \end{aligned} \tag{24}$$

Thus the phase of the outgoing wave depends upon the distance between the short circuits and the coupler and can, therefore, be adjusted by moving the short circuits. A word must be said about the phase of the outgoing wave. The scattering matrix given for the Riblet coupler makes an assumption about the reference planes at which the S parameters are measured. These reference planes may not (and most

Table 3

Location	**Port 1**	**Port 2**	**Port 3**	**Port 4**
Entering	E_0	0	0	0
Leaving	0	$E_0/\sqrt{2}$	0	$j\,E_0/\sqrt{2}$
Entering	0	$-j\,e^{j\phi}\,e^{j\Delta\phi}\,E_0/\sqrt{2}$	0	$-j\,e^{j\phi}\,e^{j\Delta\phi}\,E_0/\sqrt{2}$
Leaving	$-j\,e^{j\phi}\,E_0\,\sin\Delta\phi$	0	$-j\,e^{j\phi}\,E_0\,\cos\Delta\phi$	0

likely do not) correspond to the actual bounding planes of the physical coupler. Thus there are some phase shifts in waves moving through the coupler that have not been properly taken into account, so that the ϕ was to account for the electrical phase to the 'load' and back must be modified to take into account a fixed phase shift due to electrical lengths in the coupler. In the following analyses what matters is in fact the relative change in phases, so that an overall constant phase need not concern us, and we continue to disregard common constant phases.

What is done in practice to make a practical phase shifter is to make up movable shorts in parallel waveguides attached to the short-slot hybrid coupler, to locate the shorts the same distance from the coupler, and to gang them mechanically so that they move together. The ganged combination is then moved in and out to accomplish a phase shift linear with distance moved. In high-power systems this movement is commonly accomplished by a motorized drive mechanism. Commercially available phase shifters of the type described here have typical performance characteristics over the waveguide band of VSWR, less than 1.05; insertion loss, less than 0.1 dB; total phase shift available, more than 190°.

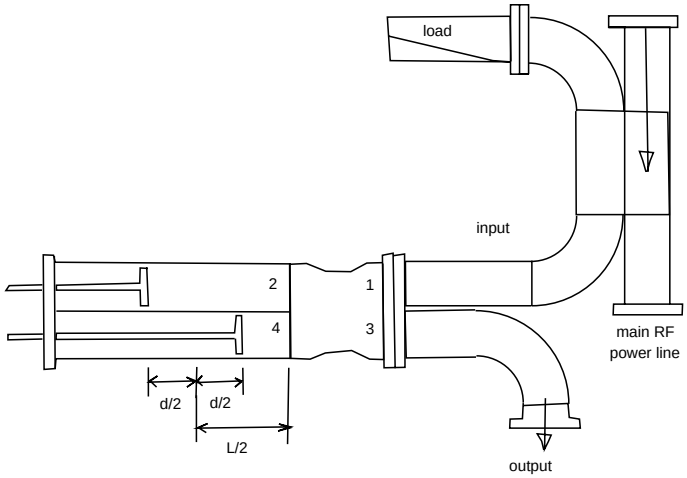

Fig. 20: Attenuator and phase shifter with reflection to the source

Two novel arrangements of Riblet couplers to produce a phase shifter/attenuator combination have been described by Ohsawa *et al.* [9] of KEK. If one can tolerate reflection back to the source, the first arrangement is very simple, as shown in Fig. 20. The arrangement consists of the two sliding shorts as in the phase shifter, but in this arrangement the location of one short is further from the phase shifter position by a distance $d/2$, say, while the other short is closer than the phase shifter position by the same amount. Thus the phase of the wave reflected from the more distant short and arriving back at the coupler is given by $\phi + \Delta\phi$, where $\Delta\phi = d/\lambda_g$, while the phase of the reflection from the nearer short is given by $\phi - \Delta\phi$. An analysis similar to that given for the power distribution system above shows the result of the differential shift $\Delta\phi$ (Table 3).

Notice, as a check, that if $\Delta\phi = 0$ we obtain the result for the straight phase shifter. Thus

Table 4: Action of the attenuator and phase shifter with load isolation

Top coupler	**Port 1**	**Port 2**	**Port 3**	**Port 4**
Entering	E_0	0	0	0
Leaving	0	$E_0/\sqrt{2}$	0	$j\,E_0/\sqrt{2}$
Bottom coupler	**Port 1**	**Port 2**	**Port 3**	**Port 4**
Entering	$j\,e^{j\phi}\,e^{-j\Delta\phi}\,E_0/\sqrt{2}$	0	$j\,e^{j\phi}\,e^{j\Delta\phi}\,E_0/\sqrt{2}$	0
Leaving	0	$j\,e^{j\phi}\,E_0\,\sin\Delta\phi$	0	$j\,e^{j\phi}\,E_0\,\cos\Delta\phi$

the differential distance d between the two sliding shorts controls the amplitude of the output (port 3), multiplying the input amplitude by $\cos\Delta\phi$, while at the same time generating a reflection directed back to the input, with amplitude $\sin\Delta\phi$ times the input amplitude. This configuration thus gives independent control of amplitude and phase; the mean position of the two shorts controls the overall phase shift and the difference in positions controls the amplitude. In the KEK application this attenuator/phase shifter was used for a prebuncher, which did not need particularly high power, and the input power was derived from the main RF power distribution system via a 20 dB directional coupler. Because of the directional coupler, at most 1/10,000th of the input power could be reflected back to the klystron.

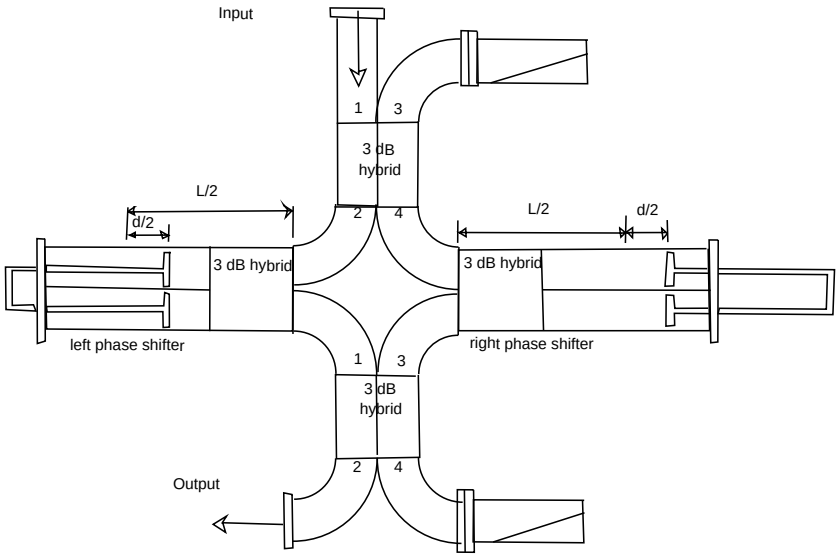

Fig. 21: Attenuator and phase shifter with load isolation

The second configuration of couplers to produce independent phase and amplitude controls reported by the staff of KEK involves the use of four Riblet couplers and completely isolates the power source from the load(s). Figure 21 shows the configuration; the top coupler splits the power equally, the left coupler is configured as a phase shifter with phase shift $\phi - \Delta\phi$, the right coupler is a phase shifter with phase shift $\phi + \Delta\phi$, and the bottom coupler recombines the power. Table 4 describes the action of the device. As before, phase shifts that are common to all signal paths are ignored. Thus once again we have independent controls on amplitude and phase; the phase shift common to both phase shifters controls the overall phase shift, while the difference in phase between the two phase shifters controls the amplitude of the output (either port 2 or port 4 of the bottom coupler).

6 NON-RECIPROCAL DEVICES

The need to isolate sources from the reflections caused by mismatched loads historically prompted the development of non-reciprocal devices at microwave frequencies. The post-war availability of ferrites, with their low electrical conductivity and high permeability, as discussed by Caspers [5], made such devices possible.

The basic property of ferrites used in non-reciprocal microwave devices is the ferrimagnetic resonance, in which the spinning electrons of the ferrite interact strongly with circularly polarized RF magnetic fields at a frequency approximately given by

$$f_{\mathrm{L}} = \frac{e}{2\pi m_{\mathrm{e}}} B \ , \tag{25}$$

where m_{e} is the mass of the electron and B is the strength of the magnetic field. The factor in front of B is approximately 2.8 MHz/G in practical units. In a waveguide one finds circularly polarized RF H fields at a particular distance from the side wall. Referring to Appendix B, where expressions for the RF magnetic fields of the H_{10} waveguide mode are given, we see that if we require that the magnitude of H_z equals that of H_x, this requirement can be met if the condition

$$\sin \frac{\pi x}{a} = \frac{\pi}{\beta a} \cos \frac{\pi x}{a} \tag{26}$$

is met. This condition becomes

$$\tan \frac{\pi x}{a} = \frac{\pi}{\beta a} = \frac{1}{\sqrt{(f/f_{\mathrm{c}})^2 - 1}} \ . \tag{27}$$

At the centre of the waveguide band, where $f = 1.5\ f_{\mathrm{c}}$, this condition yields $x = 0.232a$, i.e. the position at which circularly polarized RF magnetic fields are found is nearly half-way between the side wall and the centre of the waveguide. Thus if a piece of magnetized ferrite with biasing B field chosen for resonance at the waveguide operating frequency is placed in this location, there will be a strong interaction between the RF wave and the spins of the ferrite, for *waves travelling in one direction*. For waves travelling in the opposite direction, the sense of the circular polarization is opposite, and only a weak interaction results. Isolators use just this principle of operation, namely a slab of ferrite with a biasing magnetic field placed in the position of circular polarization, such that waves travelling in one direction are passed with minimal interaction, while those travelling in the opposite direction are strongly absorbed due to the resonant interaction. Figure 22(a) shows the arrangement of an isolator of this kind. The device passes power in one direction with very little loss but with a loss of 20 dB or more in the opposite direction. In moing to high-power operation, it becomes necessary to remove the heat from the ferrite, and designs to do this place the ferrite in maximum contact with the metallic walls of the waveguide, as shown in Fig. 22(b).

Although isolators are used to protect klystrons from reflections (the Los Alamos FEL linac has an isolator at the output of each klystron), it has become more common in high-power systems to use a circulator, since the reflected power is sent to a load rather than dissipated in the ferrite. Circulators come in four-port and three-port varieties. The four-port varieties use Riblet couplers or magic tees to divide the power, and then waveguide sections with low-loss non-reciprocal phase shifts totalling 180° carry the power to a second magic tee or Riblet coupler. The low-loss operation of the non-reciprocal phase shifters results from operating some distance from the resonance of the ferrite spins, where one still has significant interaction with the resonance but minimal loss.

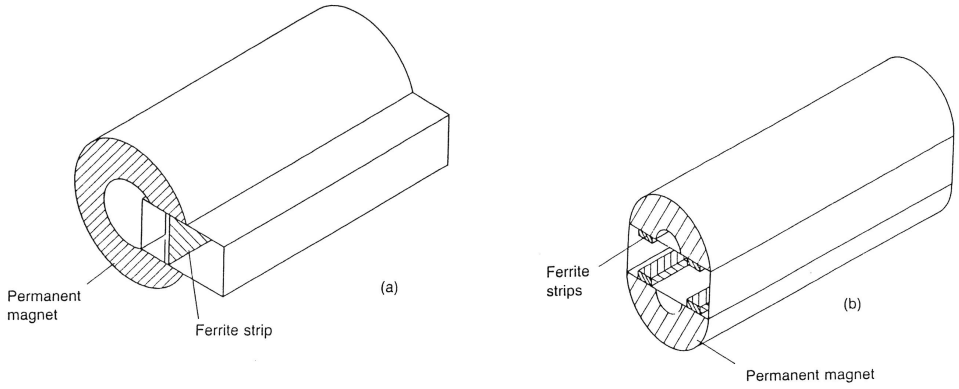

Fig. 22: Outline drawings of ferrite isolators

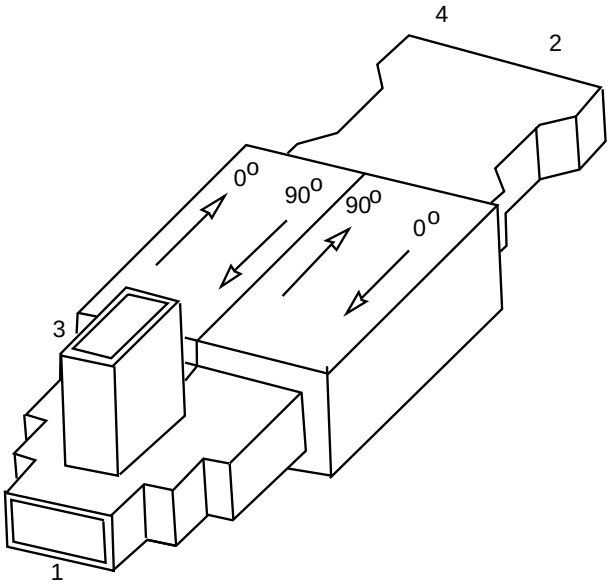

Fig. 23: A four-port (phase shift) circulator

Figure 23 shows a circulator based on a Riblet coupler and a folded magic tee. A commercial isolator of this design made for operation at 2856 MHz has the following characteristics: 10 MHz bandwidth, peak power rating 6 MW, average power rating 6 kW, 0.3 dB maximum insertion loss, 25 dB minimum isolation, VSWR less than 1.10. This water-cooled unit weighs 49 pounds (22.25 kg). A commercially available four-port circulator using two Riblet couplers and operating at 500 MHz has the following characteristics: 10 MHz bandwidth, 0.15 dB insertion loss, 20 dB minimum isolation, 4 MW CW maximum forward power, 600 kW CW maximum reflected power, VSWR less than 1.10. This water-cooled circulator weighs 6000 kg.

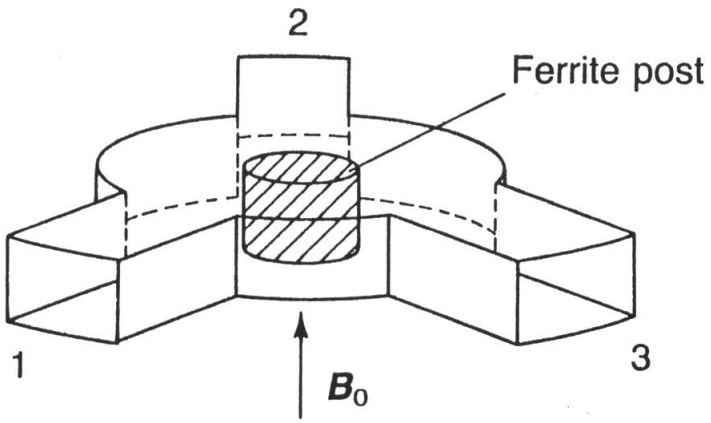

Fig. 24: Arrangement of a ferrite junction circulator

Three-port circulators are typically made with three waveguides symmetrically placed about a circular ferrite disk or stack of disks, as shown in Fig. 24. If one imagines the disks as constituting a resonator that supports the E_{110} circular cavity mode, then the ferrite disks when biased will split the two-fold degeneracy of this mode into modes having positive and negative circular polarization. The RF frequency of operation is then chosen to be midway between the resonant frequency of the positive and negative circularly polarized modes. This driving of the resonant modes off resonance produces a standing wave that couples the input port to only one of the two other ports. A commercially available three-port circulator designed for use at 352.2 MHz has the following characteristics: 10 MHz bandwidth, 0.15 dB maximum insertion loss, 20 dB minimum isolation, 1.2 MW CW maximum forward power, 600 kW CW maximum reflected power, VSWR less than 1.2. This water-cooled circulator weighs 1800 kg. Figure 25 shows part of the high-power waveguide of the CERN LEP system with a three-port circulator in the foreground. Note that the connections to the circulator are made in reduced-height waveguide.

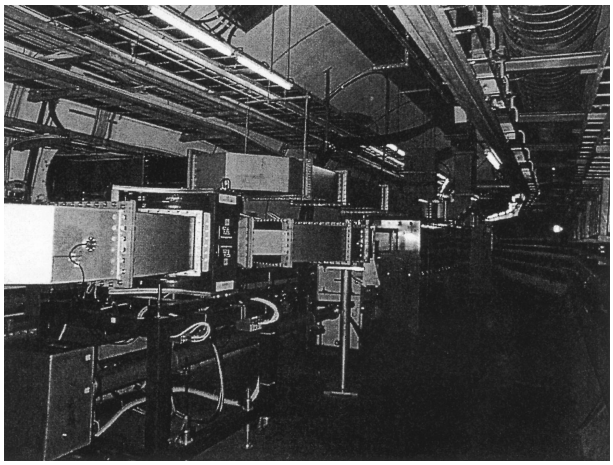

Fig. 25: View of a high-power waveguide system with a ferrite junction circulator in the foreground.

ACKNOWLEDGEMENTS

We would like to thank J.N. Weaver of SLAC for his enthusiastic help in gathering material for this article. Brian Taylor of the Lawrence Berkeley Laboratory was also most helpful. We would also like to thank George Spalek of LANL for his many discussions on RF practice. Finally we would like to thank Jean Browman for her enthusiastic attention to the subject and assistance with the preparation of materials for this work. Colleagues in the RF areas of the Accelerator Technology Division of LANL and the SRS department of the CLRC Daresbury Laboratory have been most helpful in providing material.

APPENDIX A: TEM MODE IN COAXIAL LINE

For a coaxial line with inner radius a and outer conductor radius b, the electric and magnetic fields of the dominant TEM mode are given by

$$E_{\rm r}(r,z,t) = E_0\,\frac{a}{r}\,\cos(\omega t - \beta z)\ \ , \tag{A.1}$$

$$H_\phi(r,z,t) = -\frac{E_0}{\zeta_0}\,\frac{a}{r}\,\cos(\omega t - \beta z)\ \ , \tag{A.2}$$

where ζ_0 is the characteristic impedance of free space. Corresponding to these field quantities one can calculate the integrated quantities of voltage and current (with a somewhat cavalier treatment of algebraic sign):

$$V_r(z,t) = \int_a^b E_r(r,z,t)\,{\rm d}r = E_0\,a\,\log\left(\frac{b}{a}\right)\,\cos(\omega t - \beta z) \tag{A.3}$$

and

$$I(z,t) = \int_0^{2\pi} H_\phi(a,z,t)\,{\rm d}\phi = 2\pi\,a\,\frac{E_0}{\zeta_0}\,\cos(\omega t - \beta z)\ \ , \tag{A.4}$$

where the voltage and the current on the inner conductor are positive for positive E_0.

Taking the ratio of V to I yields the characteristic impedance of the coaxial line

$$Z_{\rm c} = \frac{\zeta_0\,\log(b/a)}{2\pi}\ \ . \tag{A.5}$$

The Poynting vector for this mode is

$$\vec{S}(r,z,t) = \vec{E}\times\vec{H} = \frac{E_0^2}{\zeta_0}\,\left(\frac{a}{r}\right)^2\,\cos^2(\omega t - \beta z)\,\hat{z}\ \ . \tag{A.6}$$

Integrating over the cross sectional area of the coaxial line gives the power flowing at each longitudinal value as a function of time:

$$\begin{aligned} P(z,t) &= \int_a^b r{\rm d}r\int_0^{2\pi}{\rm d}\phi\,S_z = \\ &= \frac{E_0^2\,a^2}{\zeta_0}\,2\pi\,\log\left(\frac{b}{a}\right)\,\cos^2(\omega t - \beta z) \\ &= V(z,t)\,I(z,t)\ \ . \end{aligned} \tag{A.7}$$

so that the relationship between the maximum electric field strength E_0 and the average power transmitted in the coaxial line is

$$\bar{P} = \frac{E_0^2\, a^2}{\zeta_0}\, \pi\, \log\left(\frac{b}{a}\right) \quad . \tag{A.8}$$

If the inner conductor is made of a material with conductivity σ_a, and δ_a is the skin depth, then R_a is the surface resistance $(\sigma_a \delta_a)^{-1}$ of the inner conductor, so the power dissipated in this conductor in a length $\lambda_g = 2\pi/b = \lambda_0 = c/f$ is

$$\begin{aligned} P &= R_{\rm a} \int_0^{\lambda_{\rm g}} 2\pi a {\rm d}z H_\phi^2 \\ &= R_a\, 2\pi\, a \frac{E_0^2}{\zeta_0^2} \int_0^{\lambda_g} \cos^2(\omega t - \beta z)\, {\rm d}z \\ &= \frac{\pi a \lambda_{\rm g} R_{\rm a} E_0^2}{\zeta_0^2} \end{aligned} \tag{A.9}$$

which is independent of time. Thus the power dissipated per unit length in the inner conductor is

$$\left.\frac{{\rm d}P}{{\rm d}z}\right|_{\rm inner} \approx \frac{P}{\lambda_{\rm g}} = \frac{\pi a R_{\rm a} E_0^2}{\zeta_0} \propto \omega^{1/2} \tag{A.10}$$

The outer conductor may be made of a material different from that of the inner conductor. For example, the inner conductor is most often made of copper, while the outer conductor may be made of aluminum to save weight (at a slight increase in attenuation per unit length). If the conductivity of the outer conductor is σ_b, the power dissipated per unit length turns out to be

$$\begin{aligned} \left.\frac{dP}{dz}\right|_{\rm inner} \approx \frac{P}{\lambda_{\rm g}} &= \pi\, b \frac{a^2}{b^2}\, R_{\rm b}\, \frac{E_0^2}{\zeta_0^2} \\ &= \frac{R_{\rm b}}{R_{\rm a}} \left(\frac{a}{b}\right) \left.\frac{dP}{dz}\right|_{\rm inner} \quad . \end{aligned} \tag{A.11}$$

To calculate the attenuation constant for this TEM mode we must divide the power dissipated per unit length by the power being transmitted:

$$\alpha = \frac{1}{2\bar{P}} \frac{{\rm d}P}{{\rm d}z} = \frac{1}{2\zeta_0 \log(a/b)} \left[\frac{R_{\rm a}}{a} + \frac{R_{\rm b}}{b}\right] \quad . \tag{A.12}$$

This attenuation constant agrees with that given by Marcuvitz [10].

APPENDIX B: DOMINANT MODE IN A RECTANGULAR WAVEGUIDE

The fields of the H_{10} (TE_{10}) mode in a rectangular waveguide [width a and height b (usually $b = a/2$)] are given by

$$E_{\rm y}(x,y,z,t) = E_0\, \sin\frac{\pi x}{a}\, \cos(\omega t - \beta z) \tag{B.1}$$

$$H_{\rm x}(x,y,z,t) = -\frac{E_0}{Z_{\rm H}}\, \sin\frac{\pi x}{a}\, \cos(\omega t - \beta z) \tag{B.2}$$

$$H_{\rm z}(x,y,z,t) = -\frac{\pi/a}{\beta}\, \frac{E_0}{Z_{\rm H}}\, \cos\frac{\pi x}{a}\, \sin(\omega t - \beta z) \quad , \tag{B.3}$$

where $\beta^2 = (k^2 - (\pi/a)^2)$, $k = \omega/c$, and

$$Z_{\rm H} \equiv \frac{\omega\mu_0}{\beta} = \frac{k\zeta_0}{\beta} = \zeta_0/\sqrt{1-(f_{\rm c}/f)^2} \ , \tag{B.4}$$

where $f_{\rm c}$ is the waveguide cut-off frequency. The Poynting vector for this mode is

$$\vec{S}(x,y,z,t) = \vec{E} \times \vec{H} = \frac{E_0^2}{Z_{\rm H}} \sin^2\frac{\pi x}{a} \cos^2(\omega t - \beta z)\,\hat{z} \tag{B.5}$$

When integrated over the cross section of the guide the power transmitted as a function of z and t is:

$$P(z,t) = \int_0^b {\rm d}y \int_0^a {\rm d}x\, S_z = \frac{E_0^2}{2Z_{\rm H}}\, ab\, \cos^2(\omega t - \beta z) \ , \tag{B.6}$$

which, when averaged over time, gives the relationship between average power and maximum electric field strength,

$$\bar{P} = \frac{E_0^2}{4Z_{\rm H}}\, ab \ . \tag{B.7}$$

The power dissipated on one side wall in a guide wavelength, $\lambda_{\rm g}$, is

$$\begin{aligned} P_{\rm side} &= R_{\rm s} \int_0^b {\rm d}y \int_0^{\lambda_g} {\rm d}z\, H_{\rm z}^2(a,y,z,t) \\ &= R_{\rm s}\, b\, \frac{E_0^2}{Z_{\rm H}^2} \left(\frac{\pi/a}{\beta}\right)^2 \int_0^{\lambda_g} \sin^2(\omega t - \beta z){\rm d}z \\ &= \frac{\lambda_{\rm g} b}{2} R_{\rm s} \frac{E_0^2}{Z_H^2} \left(\frac{\pi/a}{\beta}\right)^2 = \frac{\lambda_{\rm g} b}{2} R_{\rm s} \frac{E_0^2}{\zeta_0^2} \left(\frac{\pi/a}{k}\right)^2 \\ &= \frac{\lambda_{\rm g} b}{2} R_{\rm s} \frac{E_0^2}{\zeta_0^2} \left(\frac{\lambda}{\lambda_{\rm c}}\right)^2 \ , \end{aligned} \tag{B.8}$$

which is not a function of time. In this last equation λ_c is the cut-off wavelength of the guide. Note that this loss component, arising from transverse wall currents, decreases with increasing frequency as $\omega^{-3/2}$. The power dissipated in a length $\lambda_{\rm g}$ in the top wall is

$$\begin{aligned} P_{\rm top} &= R_{\rm s} \int_0^a {\rm d}x \int_0^{\lambda_g} {\rm d}z \left(H_{\rm z}^2(a,y,z,t) + H_{\rm x}^2(x,b,z,t)\right) \\ &= R_{\rm s} \frac{E_0^2}{Z_{\rm H}^2} \int\int \Big[\left(\frac{\pi/a}{\beta}\right)^2 \cos^2\left(\frac{\pi x}{a}\right) \sin^2(\omega t - \beta z) + \sin^2\left(\frac{\pi x}{a}\right) \cos^2(\omega t - \beta z)\Big] {\rm d}x\, {\rm d}z \\ &= R_{\rm s} \frac{E_0^2}{Z_{\rm H}^2} \frac{a\lambda_g}{4} \Big[\left(\frac{\pi/a}{\beta}\right)^2 + 1\Big] = R_{\rm s} \frac{E_0^2}{Z_{\rm H}^2} \frac{a\lambda_{\rm g}}{4} \left(\frac{k^2}{\beta^2}\right) \\ &= \frac{a\lambda_{\rm g}}{4} R_{\rm s} \frac{E_0^2}{\zeta_0^2} \ . \end{aligned} \tag{B.9}$$

The power dissipated in a length $\lambda_{\rm g}$ includes that dissipated in the top and bottom walls and the two side walls,

$$P = 2 \times \lambda_{\rm g}\, R_{\rm s} \frac{E_0^2}{\zeta_0^2} \Big[\frac{a}{4} + b \left(\frac{\lambda}{\lambda_c}\right)^2\Big] \ . \tag{B.10}$$

Thus the power dissipated per unit length is

$$\frac{{\rm d}P}{{\rm d}z} \approx \frac{P}{\lambda_{\rm g}} = R_{\rm s} \frac{E_0^2}{\zeta_0^2} \Big[\frac{a}{4} + b \left(\frac{\lambda}{\lambda_c}\right)^2\Big] \ . \tag{B.11}$$

For the usual case in practice, $b = a/2$, so that the power dissipated per unit length is

$$\frac{\mathrm{d}P}{\mathrm{d}z} = R_\mathrm{s}\,\frac{a}{2}\,\frac{E_0^2}{\zeta_0^2}\left[1 + \left(\frac{\lambda}{\lambda_\mathrm{c}}\right)^2\right] \ . \tag{B.12}$$

The surface resistance R_s, being inversely proportional to the skin depth, increases as the square root of the frequency, while the quantity inside the brackets decreases with increasing frequency. Note that the contribution to the loss per unit length attributable to the transverse wall currents (arising from H_z) decreases with increasing frequency as $\omega^{-3/2}$, while that contribution from the longitudinal currents (arising from H_x) increases with increasing frequency as $\omega^{1/2}$ (for $\omega \ll \omega_c$). This observation suggests that a mode inducing only transverse wall currents would have wall losses that decrease with increasing frequency. Such a mode is the H_{01} (TE_{01}) mode in circular waveguide. This mode has been the subject of considerable attention for many years for its potential for low-loss transmission. The fact that it is a higher order mode means that any imperfection in the waveguide will result in energy being converted from the desired H_{01} mode into other propagating modes, thus providing an energy loss mechanism other than Joule heating.

Finally, the attenuation constant is calculated by taking the ratio of the power dissipated per unit length to the power being transmitted (for the case $b = a/2$),

$$\alpha = \frac{1}{2\bar{P}}\frac{\mathrm{d}P}{\mathrm{d}z} = \frac{2R_\mathrm{s}\left[1 + (f_\mathrm{c}/f)^2\right]}{a\zeta_0\sqrt{1-(f_\mathrm{c}/f)^2}} \tag{B.13}$$

where the relation $Z_\mathrm{H} = \frac{\zeta_0}{\sqrt{1-(f_\mathrm{c}/f)^2}}$ has been used. This expression for the attenuation constant agrees with that given in Marcuvitz [10].

REFERENCES

[1] T. Moreno, *Microwave Transmission Design Data* (Dover Publications, New York, 1958) (reprint).

[2] F.E. Borgnis and C.H. Papas, *Electromagnetic Waveguides and Resonators, Handbuch der Physik, Vol. XVI, Electric Fields and Waves* Berlin, Springer-Verlag, 1958).

[3] H.A. Wheeler and H. Schwiebert, Step-twist waveguide components, *Trans. I.R.E.*, MTT-3, (1955) 44.

[4] David M. Pozar, *Microwave Engineering* (Addison-Wesley, Reading, MA, 1990), Chapter 8, section 4.

[5] F. Caspers, Basic Concepts II, these proceedings.

[6] Horst Klein, Basic Concepts I, these proceedings.

[7] A.F. Harvey, *Microwave Engineering* (Academic Press, New York, 1963).

[8] H.J. Riblet, The short-slot hybrid junction, *Proc. I.R.E.* **40** (1952) 180.

[9] S. Ohsawa *et al.*, High-Power Hybrid Attenuator and Phase-Shifter Systems, Proc. Linear Accelerator Conf., Albuquerque, New Mexico, 1990, Los Alamos document LA-12004-C.

[10] N. Marcuvitz, *Waveguide Handbook*, M.I.T. Radiation Laboratory Series vol. 10 (McGraw-Hill, New York, 1951), also IEE Electromagnetic Waves Series, 1986.